Title

Fibroblasts in heart scar tissue directly regulate cardiac excitability and arrhythmogenesis

Journal

Science, 381(6665)

ISSN

0036-8075

Authors

Wang, Yijie
Li, Qihao
Tao, Bo
et al.

Publication Date

2023-09-29

DOI

10.1126/science.adh9925

Peer reviewed

HHS Public Access

Author manuscript

Science. Author manuscript; available in PMC 2024 January 05.

Published in final edited form as:

Science. 2023 September 29; 381(6665): 1480–1487. doi:10.1126/science.adh9925.

Fibroblasts in heart scar tissue directly regulate cardiac excitability and arrhythmogenesis

Yijie Wang[1,2,3,4,5,6], **Qihao Li**[7], **Bo Tao**[1,2,3,4,5,6], **Marina Angelini**[8], **Sivakumar Ramadoss**[1,2,3,4,5,6], **Baiming Sun**[1,2,3,4,5,6], **Ping Wang**[1,2,3,4,5,6], **Yuliya Krokhaleva**[9], **Feiyang Ma**[10], **Yiqian Gu**[3,11], **Alejandro Espinoza**[3,11], **Ken Yamauchi**[4,12], **Matteo Pellegrini**[3,11], **Bennett Novitch**[4,12], **Riccardo Olcese**[8,13], **Zhilin Qu**[1], **Zhen Song**[7], **Arjun Deb**[1,2,3,4,5,6,*]

[1]Division of Cardiology, Department of Medicine, University of California Los Angeles, Los Angeles, CA 90095, USA.

[2]Cardiovascular Theme, David Geffen School of Medicine, University of California Los Angeles, Los Angeles, CA 90095, USA.

[3]Department of Molecular, Cell and Developmental Biology, University of California Los Angeles, Los Angeles, CA 90095, USA.

[4]Eli and Edythe Broad Center of Regenerative Medicine and Stem Cell Research, University of California Los Angeles, Los Angeles, CA 90095, USA.

[5]Molecular Biology Institute, University of California Los Angeles, Los Angeles, CA 90095, USA.

[6]California Nanosystems Institute, University of California Los Angeles, Los Angeles, CA 90095, USA.

[7]Peng Cheng Laboratory, Shenzhen, Guangdong 518000, China.

[8]Department of Anesthesiology and Perioperative Medicine, David Geffen School of Medicine, University of California Los Angeles, Los Angeles, CA 90095, USA.

[9]UCLA Cardiac Arrhythmia Center, David Geffen School of Medicine, University of California Los Angeles, Los Angeles, CA 90095, USA.

[10]Department of Cell and Developmental Biology, Feinberg School of Medicine, Northwestern University, Chicago, IL 60611, USA.

[*]**Corresponding author.** Requests for material and correspondence should be addressed to A.D. adeb@mednet.ucla.edu.

Author contributions:

Y.W. performed and designed experiments related to optogenetics both in vitro and in vivo, performed CRISPR-Cas9 targeting, and performed all relevant analyses; B.T., B.S., and P.W. performed animal surgeries, and B.T. recorded LV pressure tracings; S.R. performed single-nuclear sequencing; F.M analyzed nuclear sequencing data; Y.G., A.E., and M.P. assisted with data interpretation and contextualization; Y.K. advised on optical stim protocols and interpretation of electrical recordings; K.Y. and B.N. assisted in recording of calcium transients; M.A performed and designed single-cell electrophysiology experiments; M.A. and R.O. assisted in interpretation and designing of coupling experiments; Q.L., Z.S., and Z.Q. designed and performed computational simulation and analyzed simulation results; A.D. conceptualized the project, designed all experiments, supervised all data collection and optogenetic experiments, interpreted all cardiac electrical tracings, and wrote the manuscript.

Competing interests: All authors declare that they have no competing interests.

[11]Institute for Quantitative and Computational Biosciences–The Collaboratory, University of California Los Angeles, Los Angeles, CA 90095, USA.

[12]Department of Neurobiology, David Geffen School of Medicine, University of California Los Angeles, Los Angeles, CA 90095, USA.

[13]Department of Physiology, David Geffen School of Medicine, University of California Los Angeles, Los Angeles, CA 90095, USA.

Abstract

After heart injury, dead heart muscle is replaced by scar tissue. Fibroblasts can electrically couple with myocytes, and changes in fibroblast membrane potential can lead to myocyte excitability, which suggests that fibroblast-myocyte coupling in scar tissue may be responsible for arrhythmogenesis. However, the physiologic relevance of electrical coupling of myocytes and fibroblasts and its impact on cardiac excitability in vivo have never been demonstrated. We genetically engineered a mouse that expresses the optogenetic cationic channel ChR2 (H134R) exclusively in cardiac fibroblasts. After myocardial infarction, optical stimulation of scar tissue elicited organ-wide cardiac excitation and induced arrhythmias in these animals. Complementing computational modeling with experimental approaches, we showed that gap junctional and ephaptic coupling, in a synergistic yet functionally redundant manner, excited myocytes coupled to fibroblasts.

Myocardial infarction (MI) results in the formation of scar tissue that enables fibroblasts to come in close apposition to myocytes (1, 2). Fibroblasts can electrically couple with myocytes (3) and promote myocyte excitability (4–9). However, the biological relevance of electrical coupling between fibroblasts and myocytes in vivo, as a mechanism of cardiac excitability and arrhythmogenesis, has not been demonstrated. Using genetically engineered animal models, optogenetics, and computational modeling, we report that fibroblasts couple with myocytes in heart scars to directly cause cardiac excitation and arrhythmogenesis in vivo.

Optogenetic-driven depolarization of fibroblasts in scar tissue altered organ-wide cardiac excitability

To determine whether cardiac fibroblasts (CFs) in scar tissue can directly drive cardiac excitation and arrhythmogenesis, we first genetically engineered a mouse in which CFs, but not myocytes, expressed the optogenetic channel channelrhodopsin variant [ChR2(H134R)], a blue light–sensitive, nonselective cationic channel (10, 11). The expression of ChR2 only in nonexcitable fibroblasts enabled us to determine changes in cardiac excitation after optical stimulation and depolarization of CFs in vivo. The mouse was engineered by crossing animals that harbored a tamoxifen-inducible fibroblast Cre recombinase (*TCF21*MerCreMer [MCM]) with animals that have the *ChR2*-enhanced yellow fluorescent protein (*eYFP*) gene knocked into the Rosa locus downstream of a floxed STOP codon (10) [*Rosa26:ChR2(H134)-eYFP* mouse]. The *TCF21*MCM driver is specific to fibroblasts and is efficient in labeling fibroblasts in scar tissue (12–15). Consistent with published reports (14, 16), we analyzed single- nucleus transcriptomic datasets and observed *Tcf21* expression

in fibroblasts and myofibroblasts in the infarcted heart (fig. S1, A to E). Cre-mediated recombination resulted in the *ChR2* gene being expressed in CFs (*TCF21*MCM-*ChR2-eYFP* or CF-ChR2 mouse). We subjected the CF-ChR2 mouse to MI by means of permanent ligation of the left anterior descending coronary artery (Fig. 1A) (17). Tamoxifen to induce Cre recombination was administered for 5 days, starting 3 days before cardiac injury (Fig. 1A). Immunofluorescent staining of the uninjured region of the heart demonstrated expression of ChR2 (eYFP expression) only in the myocardial interstitium, which is consistent with expression by CFs, with no expression of ChR2 by cardiomyocytes (Fig. 1B). At 10 days after MI, we observed robust expression of ChR2 in the injury region, with ChR2-expressing fibroblasts in close proximity to cardiomyocytes within scar tissue (Fig. 1C). Immunostaining with fibroblast marker vimentin confirmed expression of ChR2 by CFs (Fig. 1D).

For optogenetic studies, we harvested the heart at 10 days after MI and mounted it in an isolated Langendorff organ perfusion system (Fig. 1, E and F). An optical fiber that emitted blue light (473 nm) was placed just above the scar to photonically stimulate the scar tissue (Fig. 1, E and F). A pair of bipolar microelectrodes were inserted into the uninjured myocardium at the base of the heart (remote from the scar) to record changes in cardiac electrical activity (Fig. 1, E and F). We optically stimulated the cardiac scar tissue (Fig. 1G) at different frequencies starting at 7 Hz, with a pulse duration of 10 ms. Before optical stimulation, the heart rate was ~360 beats per minute (bpm), but during optical stimulation, the heart rate increased to 420 bpm, which exactly corresponded with the frequency of optical stimulation with 1:1 concordance (each optical stimulation pulse was followed by cardiac electrical activity, and each cardiac electrogram was preceded by an optical stimulation pulse) (Fig. 1H and movie S1). After cessation of optical stimulation, the heart rate returned to its pre–optical stimulation rate (Fig. 1H). The sinus rhythm noted before stimulation was replaced by a ventricular rhythm during optical stimulation, with dissociation of atrial and ventricular electrical activity, which demonstrated that fibroblast depolarization in scar tissue was sufficient to elicit organ-wide myocyte excitation (Fig. 1, I and J). Sinus rhythm resumed after cessation of optical stimulation (Fig. 1K). Optical stimulation at 9 Hz increased the heart rate to 540 bpm (Fig. 1L), with a return to prestimulation rates after cessation of optical stimulation (Fig. 1L).

Optical stimulation of the uninjured myocardium (remote from the scar tissue) of CF-ChR2 animals did not result in any change in heart rate (Fig. 1M). This is likely because the number of TCF21-labeled ChR2-expressing cells was significantly higher in the infarcted region than in remote myocardium ($P < 0.001$) (fig. S1, F to I). Neither did the heart rate change with optical stimulation of the scar tissue of the *Cre(−)Rosa26:ChR2(H134)-eYFP* animals (Fig. 1N).

Depolarization of fibroblasts in scar tissue elicited cardiac excitation in vivo and induced arrhythmogenesis

We next investigated whether optical stimulation of scar tissue altered cardiac electrical activity and heart rate in the live animal. We subjected the CF-ChR2 animal to MI and

performed open thoracotomy on the live animal 10 days after MI. The light source was positioned directly over the scar tissue (Fig. 2A), and surface electrocardiogram (ECG) electrodes were attached to the skin of the animal to record cardiac rate and rhythm (Fig. 2A). Before optical stimulation, the ECG demonstrated a rate of 390 bpm (Fig. 2B), but upon optical stimulation at 7 Hz, the rate increased to 420 bpm, which exactly corresponded to the frequency of optical stimulation with a 1:1 concordance, with a return to prestimulation rate after cessation of optical stimulation (Fig. 2B). We next looked at the rhythm and relationship of atrial (P) and ventricular activation (QRS) complexes on the surface ECG. Sinus rhythm with normal 1:1 atrioventricular (AV) conduction before optical stimulation (Fig. 2C) was replaced by a ventricular rhythm during stimulation, with clear dissociation of atrial and ventricular electrical activity, differing atrial and ventricular rates, and altered QRS morphology (Fig. 2D). Sinus rhythm with normal 1:1 AV conduction resumed after stimulation (Fig. 2E). Optical stimulation of the uninjured region of the CF-ChR2 animal did not change heart rate (Fig. 2F), and neither did the heart rate change with optical stimulation of scar tissue of *Cre(−)Rosa26:ChR2(H134R)-eYFP* animal (Fig. 2G).

We next investigated whether increased heart rate in vivo after optogenetic stimulation of CFs was associated with increased rate of cardiac contraction or electromechanical association. We optically stimulated the scar tissue in the live animal and placed a pressure transducer through the carotid artery, into the left ventricular (LV) cavity (Fig. 2H). Optical stimulation increased the heartbeat in the live animal from 135 bpm to 240 bpm (Fig. 2I), and simultaneous pressure recordings showed 1:1 concordance between each ventricular electrogram and LV contraction, which thus confirmed an electromechanical association (Fig. 2J).

We next studied whether the depolarization of fibroblasts in scar tissues can lead to arrhythmogenesis. We optically stimulated the scar of the isolated perfused CF-ChR2 heart (day 10 after MI) at different frequencies and observed that ~40% of the hearts developed postoptical stimulation rhythm disturbances. Many of these hearts developed ventricular ectopic beats after cessation of optical stimulation, and among the hearts that demonstrated poststimulation arrhythmias, 20% had ventricular bigeminy (ventricular beats in pairs) that was sustained and lasted from 30 s to 1 min (Fig. 2K). We also observed arrhythmias in the live anesthetized animal. In a subset of animals, after cessation of optical stimulation of scar tissue, surface ECG recordings demonstrated high-grade AV conduction block (Fig. 2L). During high-grade AV block, we observed multiple atrial activation signals (P waves) and occasional ventricular activation signals (QRS complexes) with loss of normal 1:1 AV conduction (Fig. 2L). Scar tissue undergoes dynamic remodeling over months after MI (18, 19). We next examined the arrhythmogenicity of the scar tissue ~12 weeks after MI and optically stimulated perfused hearts of CF-ChR2 mice, 78 to 85 days after MI. In a subset of animals, after cessation of optical stimulation of scar tissue, there was prolonged ventricular stand-still or asystole (Fig. 2M) with complete cessation of all ventricular electrical activity (Fig. 2, N and O). Ventricular asystole likely occurred because rapid and repetitive ventricular activation from fibroblast depolarization caused high-grade or complete AV conduction block (Fig. 2L) with poor or no ventricular escape rhythm of the infarcted ventricle. These observations demonstrate that depolarization of fibroblasts in scar

tissue can result in changes in cardiac excitation and conduction, which together create a permissive environment for the occurrence of sustained arrhythmias in vivo.

Electrical coupling of fibroblasts and myocytes is not mediated by connexin 43

Connexin 43 (Cx43) is a gap junctional (GJ) protein that is the most abundant connexin in the heart, is expressed by fibroblasts in the infarcted heart, and is thought to mediate fibroblast-myocyte coupling (20, 21). To determine whether Cx43 and/or other GJ proteins mediated fibroblast-myocyte coupling, we adopted an unbiased approach. We first performed single-nucleus RNA sequencing (RNA-seq) on the injured hearts of wild-type mice 7 days after MI. *Cx43* was the predominant connexin isoform expressed by cardiomyocytes (Fig. 3A). Compared with myocytes, the degree of connexin expression in CFs was much lower, but CFs and myocytes did express *Cx43*, *Cx45*, and to a lesser extent *Cx40*. *Panx1* was the only GJ-related gene, and it was expressed more highly in CFs (Fig. 3, A and B). Immunofluorescent staining confirmed Cx43 expression in fibroblasts in scar tissue of infarcted animals (fig. S2, A to D). To determine the role of Cx43 in fibroblast-myocyte coupling, we crossed the CF-ChR2 mouse with animals that have both *Cx43* alleles floxed (22) to create Cx43CKO-CF-ChR2 (CKO, conditional knockout) animals. Animals were subjected to MI, and tamoxifen was administered for 5 days to delete Cx43 in ChR2-expressing CFs (Fig. 3C). Fibroblasts harvested from the scar tissue of Cx43CKO-CF-ChR2 hearts demonstrated ~98% reduction of *Cx43* expression compared with CF-ChR2 fibroblasts (Fig. 3D). Cx43CKO-CF-ChR2 hearts (day 10 after MI) were subjected to perfusion (Fig. 3E), and at 7 Hz of optical stimulation, the heart rate exactly corresponded to the stimulation frequency with 1:1 concordance (Fig. 3E). Electrical recordings in the Cx43CKO-CF-ChR2 animals demonstrated sinus rhythm before optical stimulation (Fig. 3F), with replacement of sinus rhythm by ventricular rhythm during stimulation (Fig. 3G) and resumption of sinus rhythm after stimulation (Fig. 3H). Optical stimulation of scar tissue at higher frequencies (9 Hz) increased cardiac electrical activity from 345 bpm to 540 bpm, which exactly corresponded to the optical stimulation frequency (Fig. 3I).

We next subjected the live Cx43CKO-CF-ChR2 animal to open thoracotomy at 10 days after MI and optically stimulated the scar tissue at 7 Hz in vivo (Fig. 3J). The surface ECG demonstrated increase in heart rate to exactly correspond with the optical stimulation frequency (Fig. 3J). Sinus rhythm (Fig. 3K) was replaced by a ventricular rhythm during optical stimulation with altered QRS morphology (Fig. 3L), which was followed by the resumption of sinus rhythm after stimulation (Fig. 3M).

Myocyte-fibroblast coupling is likely not connexin dependent

We next isolated CFs from uninjured hearts of $Cx43^{fl/fl}$ animals and transfected the CFs with a plasmid that expressed Cre recombinase, followed by transfection with a lentivirus that expressed *ChR2(H134R)-eYFP*. We confirmed the deletion of Cx43 in these cells (Cx43KO-CF-ChR2) by Western blotting compared with controls (CF-ChR2 fibroblasts) (Fig. 4A). Both the Cx43KO-CF-ChR2 fibroblasts and control fibroblasts were immortalized to prevent

primary culture–associated artifacts as previously described (15). The fibroblasts were then cocultured with neonatal rat ventricular cardiomyocytes (NRVMs), which were loaded with a calcium-sensitive rhodamine-based dye to record intracellular calcium transients (Fig. 4B) (23). Optical stimulation of fibroblasts generated calcium transients in the myocytes at a rate concordant with the frequency of optical stimulation, but the deletion of Cx43 did not affect excitation of myocytes (Fig. 4, C and D). Next, we treated a coculture of myocytes and CF-ChR2 fibroblasts with a connexinmimetic peptide, Gap 26, which behaves as a pharmacological antagonist of Cx43 and other GJ channels (24, 25). On optical stimulation, Gap26 did not affect the response rate of the myocytes to optical stimulation of fibroblasts (fig. S2E). CFs not expressing ChR2 did not excite myocytes after optical stimulation (fig. S2F).

We then explored the hypothesis that there could be functional redundancy between the connexins in mediating fibroblast-myocyte electrotonic coupling. To address this question, we subjected Cx43KO-CF-ChR2 fibroblasts to CRISPR-Cas9–mediated genome editing to sequentially delete *Cx45*, *Cx40*, and *Panx1*. Sequencing confirmed biallelic deletion of *Cx45*, *Cx40*, and *Panx1* in colonies of CFs isolated from single-cell clones after CRISPR-Cas9 targeting (fig. S3, A to C). ChR2-expressing CFs deficient in *Cx40/43/45* and *Panx1* were then cocultured with NRVMs, but myocytes were excited at a rate that corresponded to the optical stimulation frequency despite the lack of these connexins (Fig. 4E).

Mathematical modeling demonstrates synergy and functional redundancy between GJ and non-GJ (ephaptic) coupling of fibroblasts and myocytes

We next performed mathematical modeling to examine the feasibility of non-GJ mediated mechanisms of myocyte-fibroblast coupling. Ephaptic coupling is a form of non-GJ coupling that has been proposed as a mechanism of propagation of the depolarization wave across the heart (26, 27). Ephaptic coupling or electric field coupling occurs when rapid changes of ionic current in a junctional cleft after depolarization of one cell can lead to membrane depolarization of the adjacent cell across the cleft (28). We adapted computational models of ephaptic and GJ coupling (fig. S4) to our experimental design that involved depolarization of fibroblasts by using optogenetic means (29, 30). In our models, multiple CFs were electrically coupled to a single myocyte either through GJ (Fig. 4F) or through ephaptic coupling (Fig. 4G). To better inform our models, we first patch clamped ChR2 fibroblasts and observed the membrane potential of ChR2 fibroblasts to change approximately from −32 mV to 0 mV during optical stimulation (fig. S5, A to C). In our simulations, optical stimulation of ChR2-expressing fibroblasts led to fibroblast depolarization and myocyte depolarization either with GJ (Fig. 4H) or ephaptic mechanisms (Fig. 4I). Differences were observed in the fibroblast and myocyte membrane potential changes between ephaptic and GJ-mediated coupling, which is suggestive of differences in electrical activation between these coupling mechanisms (Fig. 4, H and I, insets).

Subsequently, we created a mathematical model to determine the relative contribution of GJ and ephaptic coupling to myocyte depolarization (Fig. 4J). The strength of the GJ coupling was represented by the GJ conductance (G_{gap}). Ephaptic coupling is critically dependent

on the cleft volume between the cell membranes of adjacent cells and so the strength of ephaptic coupling was quantified by the volume of the cleft (*vcl*) between CFs and the myocyte (Fig. 4J). When the GJ conductance is low or close to zero (Fig. 4J, red box), fibroblast-induced myocyte depolarization fails when the *vcl* is >0.2 μm^3, which suggests that, at low GJ conductance, ephaptic coupling between fibroblasts and myocytes mediates myocyte excitation. At higher GJ conductance (Fig. 4J, blue box), ephaptic coupling was not needed, which demonstrates functional redundancy. At *vcl* of ~0.2 to 0.5 μm^3 and intermediate GJ conductance (Fig. 4J, purple box), GJ and ephaptic coupling synergized to excite the myocyte. At this *vcl* range, ephaptic coupling alone failed to conduct. With decreased ephaptic coupling (larger *vcl*), conduction failed if GJ conductance was <0.3 nS. However, when both coupling mechanisms contributed, conduction was faster than with GJ alone (see sudden color change at right of purple box), which thus demonstrates synergy.

We next investigated the impact of fibroblast Na^+ channel conductance and the number of CFs for effective fibroblast-myocyte ephaptic coupling. Myocyte excitation occurred when the fibroblast Na^+ channel conductance exceeded 2 mS/cm^2, and the number of fibroblasts coupled only by ephaptic mechanisms to a myocyte exceeded four (Fig. 4K). At a similar Na^+ channel conductance, a greater number of CFs coupled to a myocyte through ephaptic mechanisms led to faster conduction (Fig. 4K). Immunostaining for fibroblasts and myocytes in infarcted hearts of CF-ChR2 animals demonstrated a significant alteration of the myocyte/fibroblast ratio in the infarcted zone compared with uninjured myocardium ($P < 0.001$), which would potentially enable greater coupling between myocytes and fibroblasts and support the proposed model (fig. S6, A to C).

In the uninjured heart, propagation of depolarization is thought to occur by means of GJs (31). Our computational model predicted that ephaptic or GJ coupling between fibroblasts and myocytes was less resilient when compared with myocyte-to-myocyte conduction through GJ. The simulation results demonstrated that the myocyte-myocyte coupling through GJ (fig. S7A) or ephaptic coupling (fig. S7B) was superior to fibroblast-myocyte coupling either through GJ (fig. S7, C and E) or ephaptic coupling (fig. S7, D and f), respectively. To test this prediction, we generated a transgenic mouse that expressed ChR2 in cardiomyocytes only (*αMHCMerCreMer* animals crossed with *Rosa26:ChR2(H134)-eYFP* animals). Tamoxifen was administered for 5 days to induce ChR2 expression in cardiomyocytes (αMHC-ChR2 animals) (fig. S8A). Perfused hearts responded to optical stimulation frequencies as high as 14 Hz, with 100% of the hearts tested exhibiting an increase in cardiac electrical activity with a 1:1 concordance (fig. S8, B to I). We subsequently infarcted these animals (fig. S8J) and optically stimulated the scar tissue of the *αMHC*-ChR2 animals (fig. S8K) and observed that a 1:1 concordance between optical stimulation and cardiac excitation could be maintained at a frequency of 11 Hz (fig. S8L), but at 14 Hz, the fraction of injured animals that were able to maintain 1:1 concordance was significantly decreased compared with the uninjured *αMHC*-ChR2 animals ($P < 0.001$) (fig. S8, M and N). However, when the scar tissue of hearts from CF-ChR2 animals was optically stimulated at progressively increasing frequencies, in contrast to the *αMHC*-ChR2 animals, the hearts did not respond to optical stimulation at 1:1 concordance at or beyond 11 Hz (fig. S8N). These experimental data suggest that fibroblast-myocyte coupling is less robust than myocyte-myocyte coupling and validates a prediction of the computational model.

Discussion

Our study showed that fibroblast-myocyte coupling in scar tissue was robust enough to elicit cardiac excitation and arrhythmogenesis in vivo after fibroblast depolarization. Even in the absence of optogenetic channels, fibroblasts are known to be depolarized by stimuli such as cell stretch, hypoxia (32), and various neurohumoral signals (3). Scar tissue is vulnerable to rapid changes in mechanical properties (15), and fibroblast compression induces membrane depolarization by activating inward currents through nonselective cation conductance (33). Our data suggest that such pathophysiological insults that cause fibroblast depolarization in scar tissue could be potentially arrhythmogenic by means of fibroblast-myocyte coupling.

Cx43 and related GJ proteins were surprisingly dispensable for myocyte-fibroblast electrical coupling. Ephaptic and GJ conductance have been proposed to contribute to electrical coupling of adjacent myocytes (28, 34), and recent simulations suggest that ephaptic coupling can occur in all areas of small extracellular space between two adjacent cells (26). Activated CFs express voltage-gated sodium channel Nav1.5 and have sodium and potassium rectifier currents similar to those recorded from myocytes, which potentially enables ephaptic coupling (35). Our study demonstrates that ephaptic and GJ coupling can act in a synergistic yet functionally redundant manner to excite myocytes, but it does not exclude other proposed coupling mechanisms such as cellular nanotubes (36) or the possibility that a connexin-like protein expressed in low abundance in scar tissue compensates for the concomitant loss of the most highly expressed GJ genes.

Our findings potentially have clinical implications for treatment of arrhythmias. Scar-related ventricular arrhythmias are treated with radio frequency catheter ablation. Ablation reduces the number of myocytes but activates fibroblasts and induces fibrosis. Approximately 50% of patients who are treated with radio frequency ablation of scar-related ventricular tachycardia have arrhythmia recurrence. Our data suggest that increased fibroblast accumulation and remodeling of the scar may create fresh coupling foci between fibroblasts and residual myocytes and lead to new substrates for arrhythmogenesis.

Supplementary Material

Refer to Web version on PubMed Central for supplementary material.

ACKNOWLEDGMENTS

We thank E. Olson (University of Texas Southwestern) for sharing the TCF21MCM mice with us. We thank G. Salama (University of Pittsburgh) for assisting with ephaptic experiments. We thank the following colleagues from UCLA: K. Shivkumar and P. Rajendran for helping us establish an optogenetic suite, B. Khakh for insights into ephaptic signaling, and J. Lusis and J. Weiss (professor emeritus) for providing helpful suggestions on the manuscript.

Funding:

This study was supported by grants from the US Department of Defense (W81XWH-20-1-0238) and the US National Institutes of Health (HL149658, HL152176, HL149687, AR075867, and DK132735 to A.D.; HL134709, HL157116, and HL139829 to Z.Q.; and HL134346 and HL152296 to R.O.), from the American Heart Association (postdoctoral fellowship 906531 to Y.W.), and from the Natural Science Foundation of China (no. 82172067 to Z.S.).

Data and materials availability:

All data are available in the manuscript or the supplementary materials. Single-nucleus RNA-seq data were deposited to the Gene Expression Omnibus database under accession number GSE235434 (https://www.ncbi.nlm.nih.gov/geo/query/acc.cgi?acc=GSE235434).

REFERENCES AND NOTES

1. Christia P. et al., J. Histochem. Cytochem. 61, 555–570 (2013). [PubMed: 23714783]
2. Frangogiannis NG, J. Clin. Invest. 127, 1600–1612 (2017). [PubMed: 28459429]
3. Mahoney VM, Mezzano V, Morley GE, Prog. Biophys. Mol. Biol. 120, 128–133 (2016). [PubMed: 26713556]
4. Nguyen TP, Qu Z, Weiss JN, J. Mol. Cell. Cardiol. 70, 83–91 (2014). [PubMed: 24184999]
5. Nguyen TP, Xie Y, Garfinkel A, Qu Z, Weiss JN, Cardiovasc. Res. 93, 242–251 (2012). [PubMed: 22049532]
6. Camelliti P, Borg TK, Kohl P, Cardiovasc. Res. 65, 40–51 (2005). [PubMed: 15621032]
7. Ongstad E, Kohl P, J. Mol. Cell. Cardiol. 91, 238–246 (2016). [PubMed: 26774702]
8. Xie Y. et al., Heart Rhythm 6, 1641–1649 (2009). [PubMed: 19879544]
9. Rog-Zielinska EA, Norris RA, Kohl P, Markwald R, Trends Mol. Med. 22, 99–114 (2016). [PubMed: 26776094]
10. Madisen L. et al., Nat. Neurosci. 15, 793–802 (2012). [PubMed: 22446880]
11. Lin JY, Exp. Physiol. 96, 19–25 (2011). [PubMed: 20621963]
12. Acharya A, Baek ST, Banfi S, Eskiocak B, Tallquist MD, Genesis 49, 870–877 (2011). [PubMed: 21432986]
13. Acharya A. et al., Development 139, 2139–2149 (2012). [PubMed: 22573622]
14. Kanisicak O. et al., Nat. Commun. 7, 12260 (2016). [PubMed: 27447449]
15. Yokota T. et al., Cell 182, 545–562.e23 (2020). [PubMed: 32621799]
16. Tallquist MD, Molkentin JD, Nat. Rev. Cardiol. 14, 484–491 (2017). [PubMed: 28436487]
17. Li S. et al., J. Clin. Invest. 132, e149711 (2022). [PubMed: 34813507]
18. Burchfield JS, Xie M, Hill JA, Circulation 128, 388–400 (2013). [PubMed: 23877061]
19. Xie M, Burchfield JS, Hill JA, Circulation 128, 1021–1030 (2013). [PubMed: 23979628]
20. Rodríguez-Sinovas A, Sánchez JA, Valls-Lacalle L, Consegal M, Ferreira-González I, Int. J. Mol. Sci. 22, 4413 (2021). [PubMed: 33922534]
21. Camelliti P, Devlin GP, Matthews KG, Kohl P, Green CR, Cardiovasc. Res. 62, 415–425 (2004). [PubMed: 15094361]
22. Liao Y, Day KH, Damon DN, Duling BR, Proc. Natl. Acad. Sci. U.S.A. 98, 9989–9994 (2001). [PubMed: 11481448]
23. Kostecki GM et al., Sci. Rep. 11, 4430 (2021). [PubMed: 33627695]
24. Hulsmans M. et al., Cell 169, 510–522.e20 (2017). [PubMed: 28431249]
25. Desplantez T, Verma V, Leybaert L, Evans WH, Weingart R, Pharmacol. Res. 65, 546–552 (2012). [PubMed: 22406236]
26. Lin J, Keener JP, IEEE Trans. Biomed. Eng. 60, 576–582 (2013). [PubMed: 23335235]
27. Kucera JP, Rohr S, Rudy Y, Circ. Res. 91, 1176–1182 (2002). [PubMed: 12480819]
28. Gourdie RG, Anat. Rec. 302, 93–100 (2019).
29. Ly C, Weinberg SH, Chaos 32, 033123 (2022). [PubMed: 35364829]
30. Morotti S, Edwards AG, McCulloch AD, Bers DM, Grandi E, Physiol J. 592, 1181–1197 (2014).
31. Eckardt D. et al., J. Mol. Cell. Cardiol. 41, 963–971 (2006). [PubMed: 16963078]
32. Kamkin A. et al., Pflugers Arch. 446, 169–174 (2003). [PubMed: 12739154]
33. Kamkin A, Kiseleva I, Isenberg G, Cardiovasc. Res. 57, 793–803 (2003). [PubMed: 12618241]

34. Veeraraghavan R, Gourdie RG, Poelzing S, Am. J. Physiol. Heart Circ. Physiol. 306, H619–H627 (2014). [PubMed: 24414064]
35. Chatelier A. et al., J. Physiol. 590, 4307–4319 (2012). [PubMed: 22802584]
36. Quinn TA et al., Proc. Natl. Acad. Sci. U.S.A. 113, 14852–14857 (2016). [PubMed: 27930302]

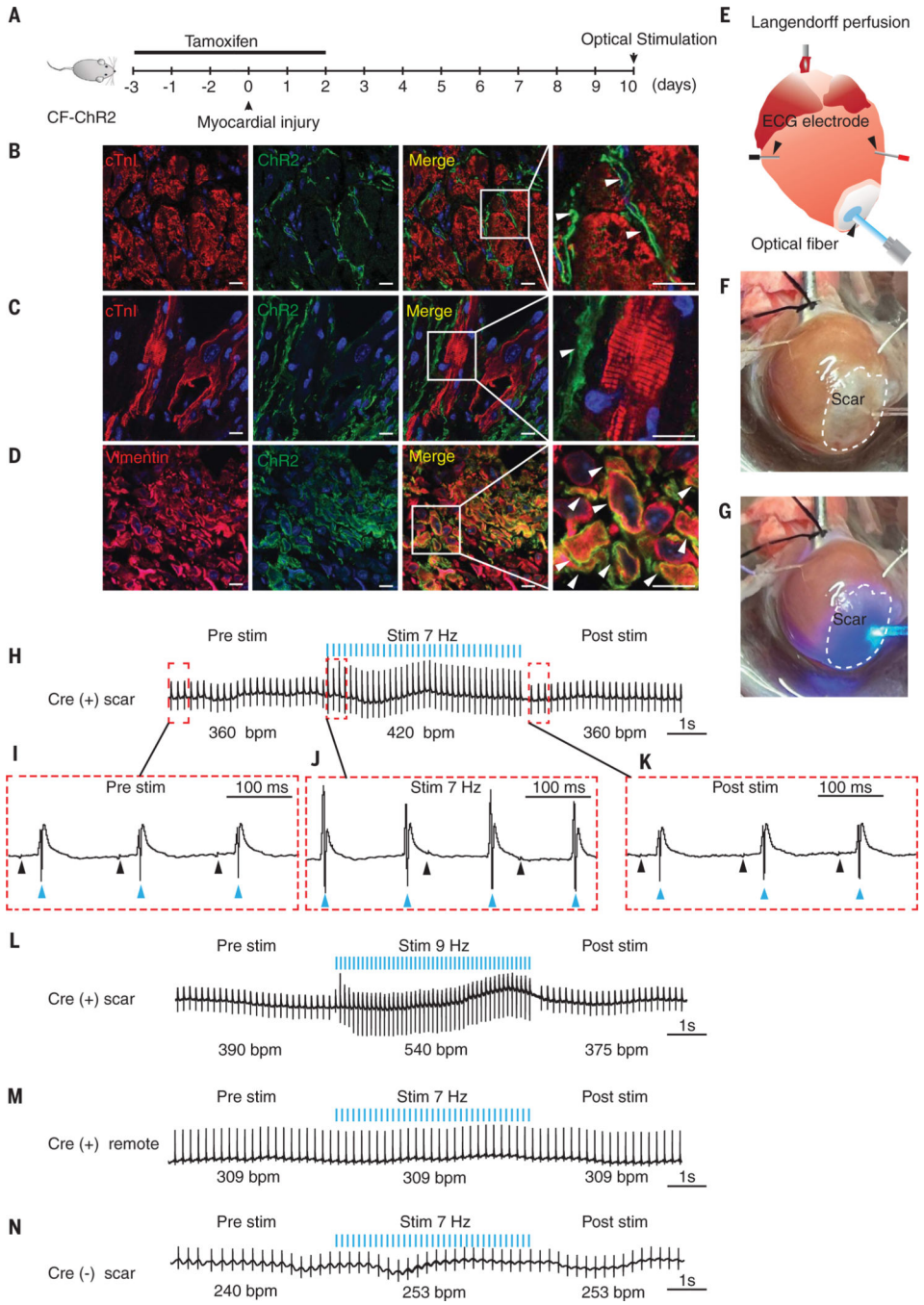

Fig. 1. Optical stimulation of scar tissue of CF-ChR2 animal drives organ-wide cardiac excitation.

(**A**) Schematic of experiment outlining administration of tamoxifen to induce Cre-mediated recombination and harvesting of heart at 10 days after MI. (**B** and **C**) Immunofluorescent staining of heart of CF-ChR2 animal harvested at 10 days after MI that demonstrates cardiomyocyte (red, Troponin I) and ChR2-expressing cells (green, eYFP) in uninjured myocardium remote to scar tissue (B) and scar tissue (C). Merged image and magnified inset demonstrating spatial relationship of fibroblasts (arrows) to myocytes. Scale bar, 20 μm. (**D**)

Immunostaining for vimentin (red) and ChR2 (green) that demonstrates colocalization of ChR2 in vimentin-expressing cells (merged image and magnified inset [arrows, yellow]). (**E** to **G**) (E) Schematic of optical stimulation of scar tissue of the per- fused heart before (F) and at the onset of (G) optical stimulation with blue light. (**H**) Cardiac electrical recording before, during, and after optical stimulation of scar tissue at 7 Hz (blue lines indicate pulses of optical stimulation, bpm: recorded cardiac electrical activity in beats per minute). (**I** to **K**) Magnified atrial (black arrows) and ventricular electrograms (blue arrows) from recordings before (I), during (J), and after (K) optical stimulation. Note the dissociation of atrial and ventricular rhythm during stimulation with atrial activation not preceding ventricular activation. (**L**) Cardiac electrical recording after optical stimulation of scar at 9 Hz. (**M** and **N**) Cardiac electric recording after stimulation of myocardium remote to scar tissue in CF-ChR2 animal (M) or scar in Cre (−) animal (N). Representative tracings shown; $n = 20$ Cre (+) scar, $n = 6$ Cre (−) scar, and $n = 10$ Cre (+) remote.

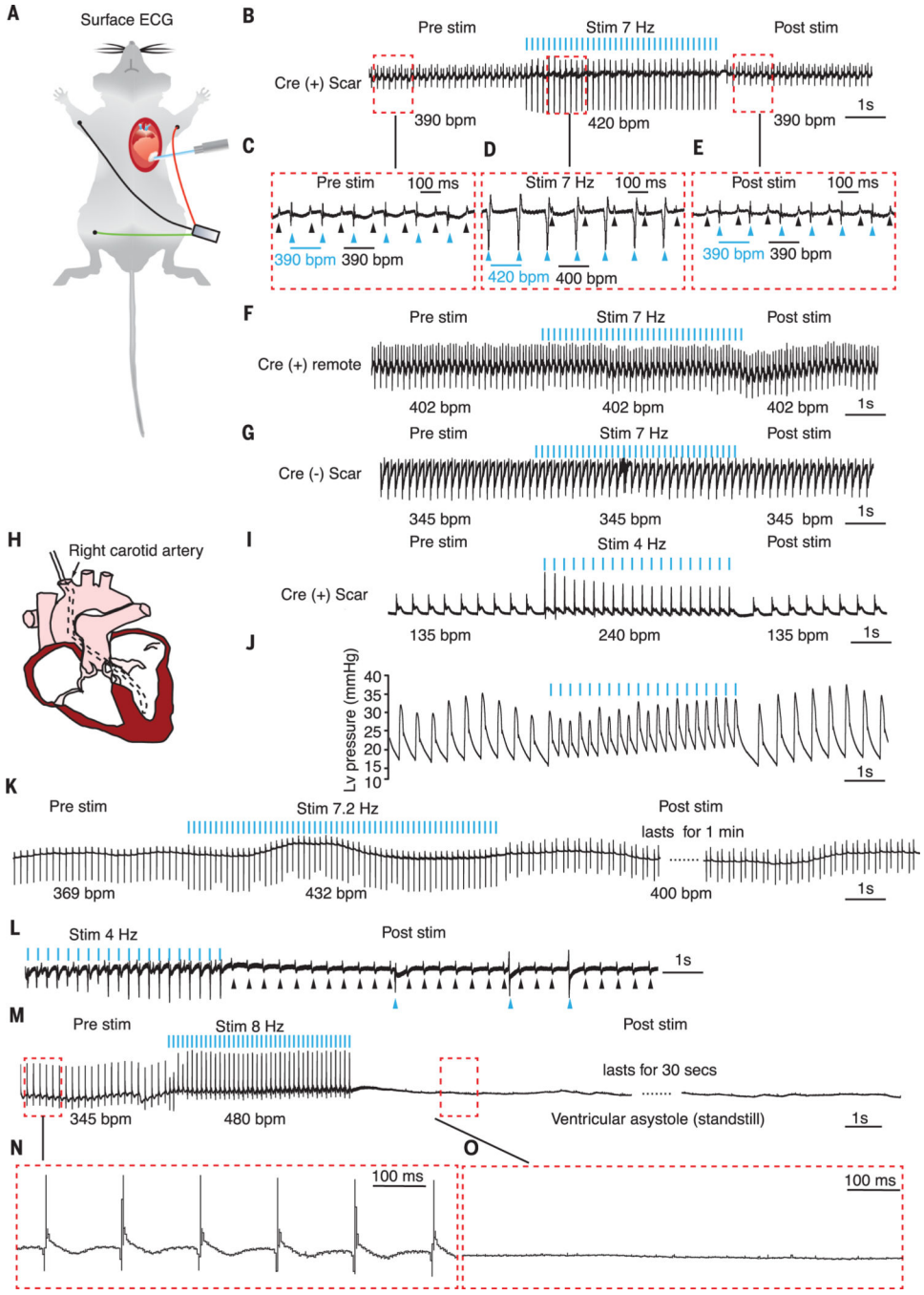

Fig. 2. Depolarization of fibroblasts in scar tissue drives cardiac excitation in vivo and induces arrhythmogenesis.

(**A**) Schematic of experiment that demonstrates anesthetized CF-ChR2 animal subjected to open thoracotomy with optical stimulation of scar tissue and simultaneous surface ECG recording by using limb leads. (B) ECG recording before, during, and after optical stimulation of scar tissue at 7 Hz (blue bars represent optical stimulation pulses). (**C** to **E**) Magnified recordings demonstrating atrial (P waves, black arrows) and ventricular activity (QRS complexes, blue arrows) from recordings before (C), during (D), and after

(E) stimulation. Note that atrial (P-P) rate and ventricular (R-R) rates are different in (D), which confirms the dissociation of atrial and ventricular rhythm during optical stimulation followed by resumption of sinus rhythm poststimulation. (**F** and **G**) Surface ECG recording after optical stimulation of myocardium remote to scar tissue (F) or scar in Cre (−) animal (G). (**H** to **J**) LV pressure recording before and after optical stimulation in live CF-ChR2 animal. (H) Technical schematic showing introduction of pressure catheter through the carotid into the LV. (I) Surface ECG demonstrating electrical activity before, during, and after optical stimulation. (J) Simultaneous recording of LV pressures (note that increased cardiac electrical activity is associated with increased frequency of synchronous beats that generate LV pressure). (**K** to **O**) Arrhythmogenesis noted in a subset of animal hearts after optical stimulation of scar tissue. (K) Electrical recording from intact perfused heart before, during, and after optical stimulation, which demonstrates ventricular bigeminy (paired beats) that was sustained for 1 min in the absence of any further perturbations. (L) Surface ECG from live animal subjected to optical stimulation of scar that demonstrates high-grade AV block. Note the loss of 1:1 conduction between atrial (P wave, black arrows) and ventricular (QRS complex, blue arrows) activity. (M to O) Heart of CF-ChR2 animal harvested 3 months after MI and subjected to optical stimulation demonstrates ventricular asystole after cessation of optical stimulation (M), and magnified view of ventricular rhythm before (N) and after (O) stimulation demonstrates absence of any ventricular rhythm poststimulation (representative tracings, $n = 15$ per group).

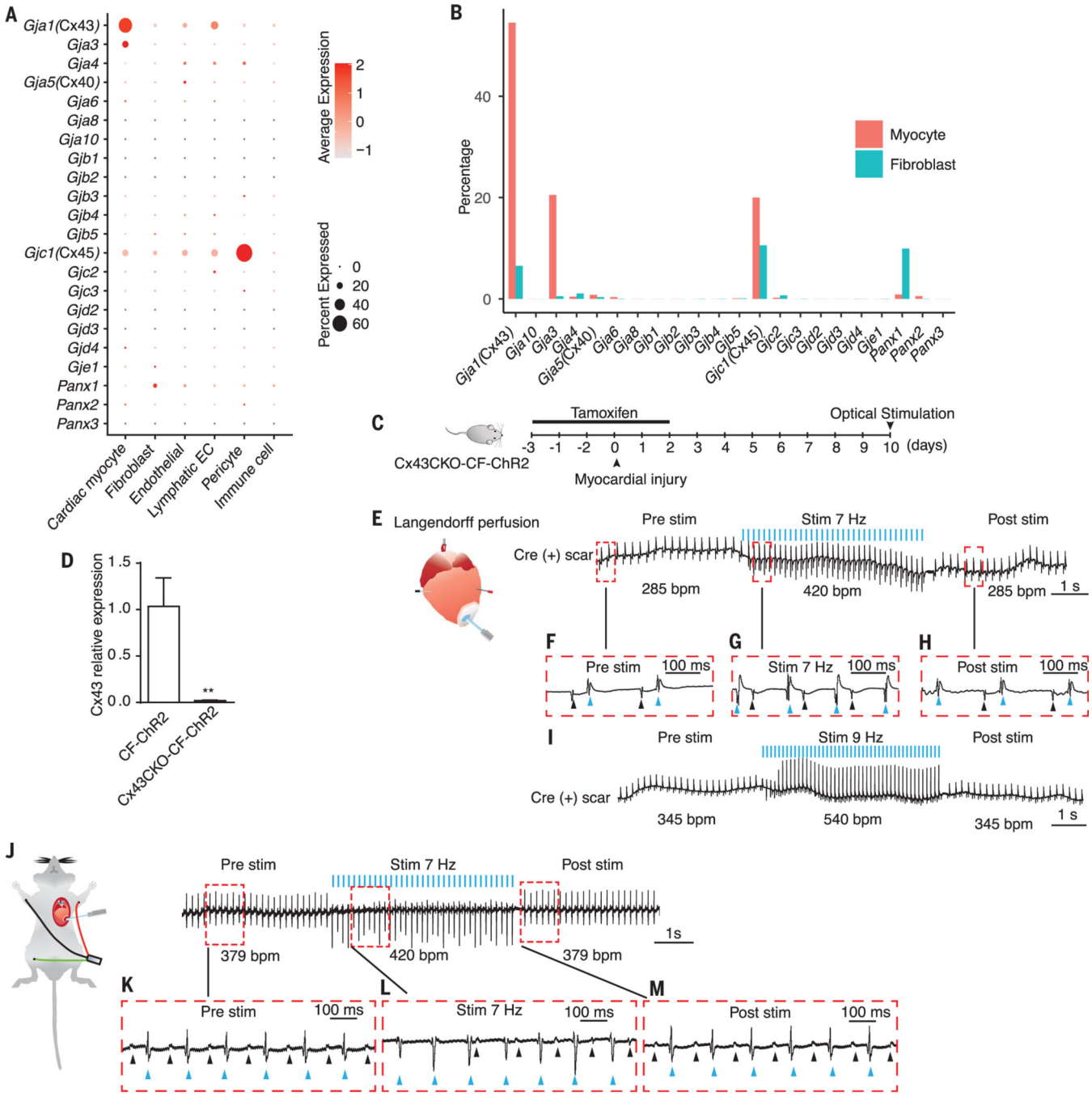

Fig. 3. Connexin 43 is not required for fibroblast-myocyte coupling in vivo.

(**A**) Dot plot from single-nuclear RNA-seq that shows gene expression of various connexins and pannexins across cardiac cell population in the heart harvested 7 days after MI. EC, endothelial cell. (**B**) Comparison of expression of connexins/pannexins in CFs and myocytes shown as a percentage of cells expressing the gene of interest. (**C**) Schematic of generation of the Cx43CKO-CF-ChR2 animal with administration of tamoxifen to induce Cre-mediated recombination. (**D**) Quantitative polymerase chain reaction (qPCR) that demonstrates *Cx43* expression in CFs from Cx43CKO-CF-ChR2 animals compared with CFs from CF-ChR2

control animals (data are represented as mean ± SD, $^{**}P < 0.01$, $n = 3$). (**E** to **H**) Intact perfused hearts of Cx43CKO-CF-ChR2 animals harvested 10 days after MI were subjected to optical stimulation of scar tissue. (E) Electrical recording of heart before, during, and after optical stimulation at 7 Hz (blue bars represent optical stimulation pulses; representative tracings, $n = 8$). (F to H) Magnified electrograms demonstrate atrial (black arrows) and ventricular activity (blue arrows) before (F), during (G), and after (H) stimulation. Note dissociation of atrial and ventricular activity during optical stimulation. (**I**) Cardiac electrical recording after optical stimulation of scar at 9 Hz. (**J** to **M**) Surface ECG of live Cx43CKO-CF-ChR2 animal subjected to optical stimulation of scar at 10 days after MI. (J) ECG recording before, during, and after stimulation at 7 Hz. (K to M) Atrial (P wave, black arrows) and ventricular (QRS complexes, blue arrows) activity before (K), during (L), and after (M) stimulation. Note dissociation of atrial and ventricular activity during stim followed by resumption of normal sinus rhythm after stimulation (representative tracings, $n = 9$ per group).

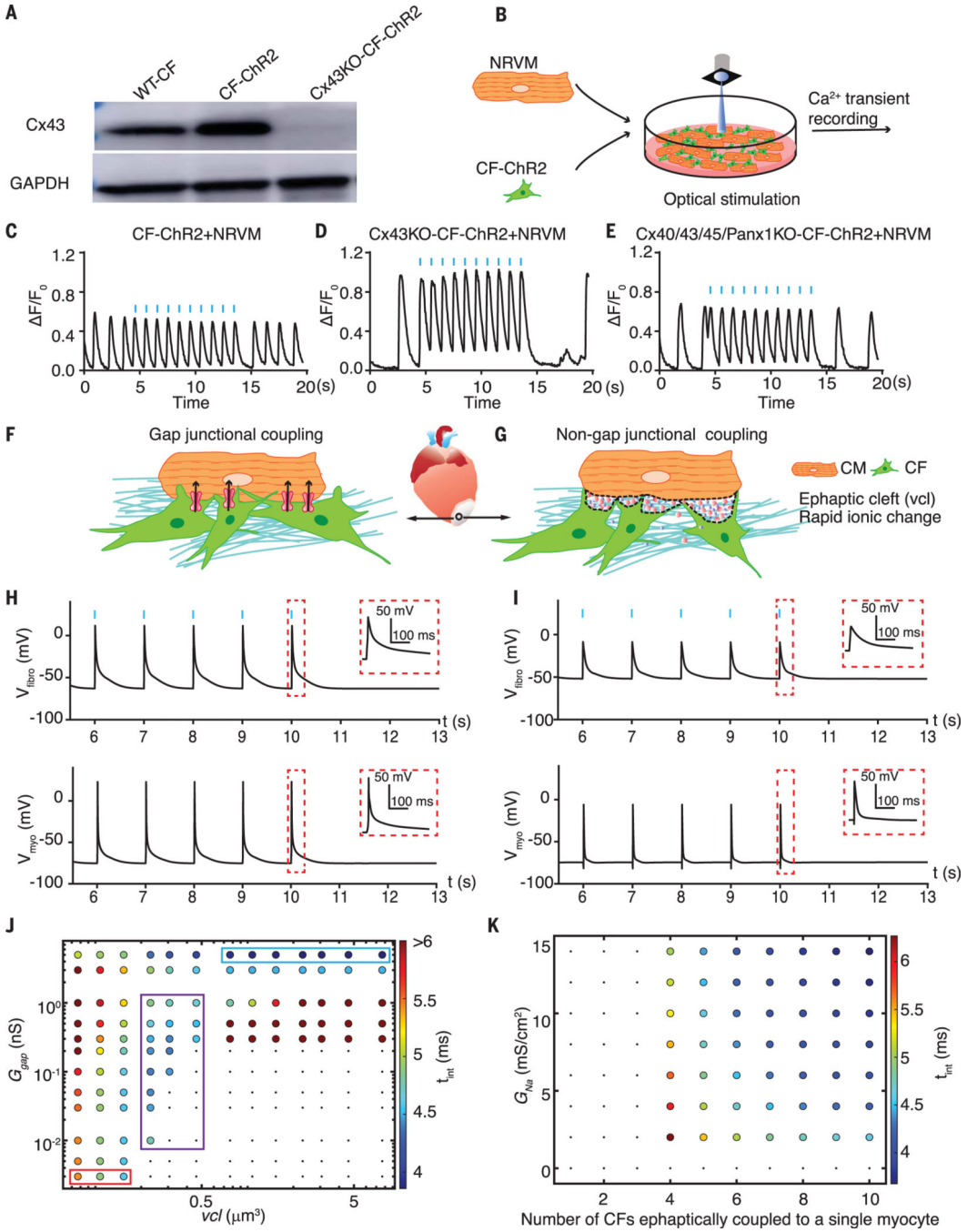

Fig. 4. Connexin-dependent GJ coupling is dispensable for fibroblast-myocyte electrical coupling.

(**A**) Western blot demonstrating expression of Cx43 in wild-type (WT) CFs, CF-ChR2 (Cx43fl/fl) CFs, and after transfection of Cx43fl/fl CFs with Cre plasmid to generate Cx43KO CFs. (**B**) Schematic of optical stimulation of CF-ChR2 cocultured with NRVMs loaded with x-Rhod-AM dye to record calcium transients. (**C** to **E**) Recording of calcium transients in cardiomyocytes after optical stimulation of CF-ChR2 (C), Cx43KO-CF-ChR2 (D), and Cx40/43/45/Panx1KO-CF-ChR2 (E) fibroblasts (blue bars represent

optical stimulation pulses). Representative tracings, $n = 5$ per group. (**F** to **K**) Modeling of GJ (F) and non-GJ (ephaptic) (G) coupling, with simulation demonstrating successful depolarization of fibroblasts (V_{fibro}) and myocytes (V_{myo}) with either GJ (H) or non-GJ (I) coupling. Blue bars indicate pulses of optical stimulation applied to fibroblasts. (H and I, insets) Differences in membrane depolarization of fibroblast and myocyte with GJ and non-GJ coupling. (J) Simulation showing myocyte excitation with variation in GJ and ephaptic coupling (*vcl*). Ten fibroblasts were connected to the myocyte for this simulation. The red box represents low GJ conductance but strong ephaptic coupling, and the blue box represents strong GJ conductance with weak ephaptic coupling. The purple box indicates where ephaptic and GJ coupling synergize to excite myocytes. (K) Simulation showing myocyte excitation with variation in Na^+ channel conductance of CFs and the number of CFs coupled to the myocyte solely through ephaptic coupling. In (J) and (K), colored circles represent successful myocyte excitation, and dots represent unsuccessful myocyte excitation. Color of the circles represents delay (time interval) to myocyte excitation t_{int} (milliseconds).